Analysis of the reverse I-V characteristics of diamond-based PIN diodes

Mehdi Saremi,[1] Raghuraj Hathwar,[1] Maitreya Dutta,[2] Franz A. M. Koeck,[3] Robert J. Nemanich,[3] Srabanti Chowdhury,[2] and Stephen M. Goodnick[1]
[1]*Department of Electrical Engineering, Arizona State University, Tempe, Arizona 85287-8806, USA*
[2]*Department of Electrical Engineering, UC Davis, Davis, California 95616, USA*
[3]*Department of Physics, Arizona State University, Tempe, Arizona 85287-8806, USA*

(Received 6 June 2017; accepted 12 July 2017; published online 25 July 2017)

Diamond is one of the most promising candidates for high power and high temperature applications, due to its large bandgap and high thermal conductivity. As a result of the growth and fabrication process of diamond-based devices, structural defects such as threading dislocations (TDs) may degrade the electrical properties of such devices. Understanding and control of such defects are important for improving device technology, particularly the reverse breakdown characteristics. Here, we show that the reverse bias current-voltage characteristics in diamond PIN diodes can be described by hopping conduction and Poole-Frenkel emission through TDs over the temperature (T) range of $323\,\mathrm{K} < T < 423\,\mathrm{K}$, for typical values of the TD density found in epitaxially grown materials. *Published by AIP Publishing.* [http://dx.doi.org/10.1063/1.4986756]

Among wide bandgap semiconductor materials such as GaN[1] and SiC,[2] diamond has potentially superior electrical and thermal properties such as high breakdown field,[3] high carrier mobility,[4] high thermal conductivity,[5,6] and extremely low intrinsic carrier concentration at room temperature. Based on these advantages, predictions of the high potential figures of merit have been made for both active devices such as field-effect transistors (FETs)[7–9] and high-power switches and passive devices such as Schottky[10] and PIN[11] diodes, especially in elevated temperature regimes.[12]

As improvements in diamond-based device technology continue in terms of appropriate growth technologies and post-annealing processes,[13–16] it is important to understand the origin of the reverse leakage current and the behavior of defects such as threading dislocations (TDs) in the reverse breakdown characteristics. Several investigations have been conducted for the leakage mechanisms of other materials such as GaN,[17,18] GaN/AlGaN/GaN heterostructures,[19–21] and InGaAs,[22] which concluded that Poole-Frenkel emission (PFE) dominates in different temperature ranges.[23] However, no investigation has been made to analyze the reverse current mechanism of diamond-based diodes to date.

In the present work, we investigate the reverse I-V characteristics of diamond-based PIN diodes fabricated on bulk diamond substrates comparing experimental data with theory. The temperature dependence of the reverse I-V characteristics suggests that the reverse current is mainly dominated by the hopping conduction mechanism at low electric fields, while PFE dominates at high electric fields. In the case of hopping conduction, the carrier energies are lower than the maximum energy of the potential barrier between two trapping sites, and carrier transport is primarily dominated by thermally assisted tunneling between sites.[24,25] However, at higher electric fields, the barrier to thermionic emission to the conduction band (for electrons)/valence band (for holes) is lowered, leading to transport dominated by PFE. Both hopping conduction and PFE mechanisms here described are attributed to carrier transport via threading dislocations in diamond, and these models are fit to experimental data over a temperature range of $323\,\mathrm{K} < T < 423\,\mathrm{K}$. The diamond growth and device fabrication, modeling methodology, temperature analysis, and results are described in the below paragraphs.

While diamond can be synthesized by various techniques, the most commonly used technology is chemical vapor deposition (CVD) of samples grown using the high pressure, high temperature (HPHT) technique. To controllably prepare the electronic grade material, i.e., intrinsic and doped diamond with a controlled impurity concentration, microwave plasma enhanced CVD (MPCVD) has emerged as the most practical approach for this type of diamond growth. In addition to control the impurity concentration for donor and acceptor dopants, homoepitaxial diamond growth is feasible using single crystal diamond substrates. With MPCVD, it is practical to prepare diamond epilayers with intrinsic, n- and p-type properties in a high purity ambient and thus realize electronic device structures. As plasma CVD diamond growth utilizes a hydrogen plasma with small amounts of methane (<2%), exposure of the diamond surface to a pure hydrogen plasma prior to growth allows us to prepare a clean surface for low defect interfaces.

The PIN structures were grown by microwave plasma enhanced chemical vapor deposition (MPCVD) dedicated deposition systems for intrinsic and doped diamond layers as discussed elsewhere.[26] Prior to diamond growth, the HPHT type IIb (111) oriented substrate was cleaned in an acid mixture (H_2SO_4:H_2O_2:H_2O:: 3:1:1) at 220 °C for 15 min to remove organic and metallic contaminants. This was followed by HF treatment for 5 min to remove SiO_2 and metallic contaminants. Finally, the sample was placed in a solution of (NH_4OH:H_2O_2:H_2O:: 1:1:5) at 75 °C for 15 min to remove any remaining particles and organic contaminants. For the i-layer growth, the base pressure was set at $\sim 10^{-8}$ Torr. The growth surface was exposed to the pure hydrogen plasma for 15 min with a hydrogen flow rate of 400 sccm, a chamber pressure of 90 Torr, and a microwave power offset of 1500 W. The growth temperature as measured using an optical pyrometer was ~1075 °C. Then, a second growth step with a microwave power of 1200 W, a chamber pressure of 60 Torr, and a methane flow rate of

0.2 sccm took place. The i-layer growth was performed for 33 h with the temperature set at ~830 °C after which gas flow was terminated and microwave power shut off. For the n-layer growth, an initial exposure to the pure hydrogen plasma for 30 min was performed with a flow rate of 400 sccm, a chamber pressure of 60 Torr, and a microwave power of 2000 W. It commenced by reducing the hydrogen flow rate to 360 sccm and establishing a methane flow rate and a 200 ppm trimethylphosphine/hydrogen flow rate of 0.5 sccm and 40 sccm, respectively. The phosphorus doped n-type diamond growth was done at 30 min with the growth temperature of ~770 °C.

The as-grown samples were first O-terminated by immersing in an acid mixture of H_2S0_4:HNO_3:: 3:1 for 30 min to remove surface conduction. The n-type contacts were patterned using standard double layer photolithography followed by metal deposition using e-beam evaporation and liftoff. The metal stack consisted of Ti/Pt/Au: 50 nm/50 nm/150 nm. Square and circular diodes with side lengths and diameters ranging from 30 μm to 280 μm were deposited without mesa isolating the devices. A common backside contact using Ti/Pt/Au: 50 nm/50 nm/300 nm which utilized the conductive 3 mm × 3 mm type-IIb substrate was used to make contact with the p-type layer. A continuous light emission in the deep ultraviolet region was observed in the forward bias of the diode, confirming bipolar transport in these devices.[27] The doping concentrations of the p- and n-type regions are 9×10^{19} cm^{-3} and 5×10^{19} cm^{-3}, respectively. The forward current density was 200 A/cm^2 at 10 V. The reverse blocking was 100 V with the current density compliance set at 1 A/cm^2.

Threading dislocations (TDs) are known to affect the electrical properties of diamond, particularly in homoepitaxial CVD synthetic diamond materials, and they influence carrier transport in diamond-based devices.[28–30] Due to the formation of multiple parallel paths as shown in Fig. 1, these dislocations may degrade the device performance of diamond-based structures through increased leakage current.

Figure 2 shows the band diagram of a PIN diode in which hopping conduction of holes is dominant at low electric fields and PFE is the dominant transport mechanism of holes at high electric fields where the red circles in Fig. 2 represent holes. It is worthwhile to mention that the n-region is easily depleted in the reverse bias because the activation energy of phosphorus dopants is high (around 0.57 eV) and the doping concentration of the n-region is not high enough (5×10^{19} cm^{-3}). Therefore, the free electron concentration in the n-region is insignificant. On the other hand, the cathode contact with the work function near the valence band of the n-region is able to inject holes into the depleted n-region at the reverse bias condition. The injected holes depending on the electric field transfer from the cathode contact to threading dislocation sites by hopping conduction and PFE for low and high electric fields, respectively.

The leakage current through TDs in other materials has previously been attributed to PFE conduction,[31–33] which describes the field emission of carriers from localized states associated with the threading dislocations into a continuum of electronic states,[31] as shown in Fig. 2(b) for the case of hole dominated transport. Since PFE occurs due to electric

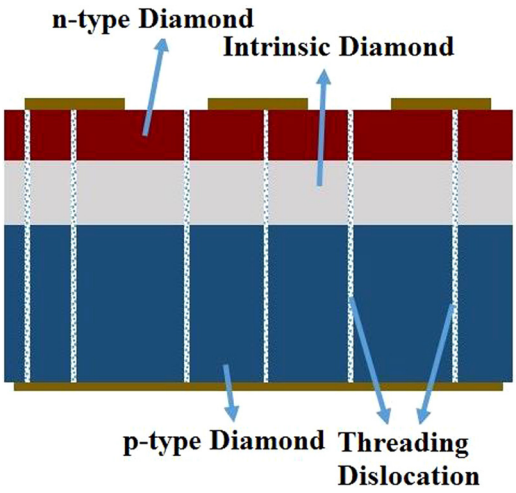

FIG. 1. Schematic diagram of a diamond-based PIN diode in which threading dislocations are shown as parallel paths across the device.

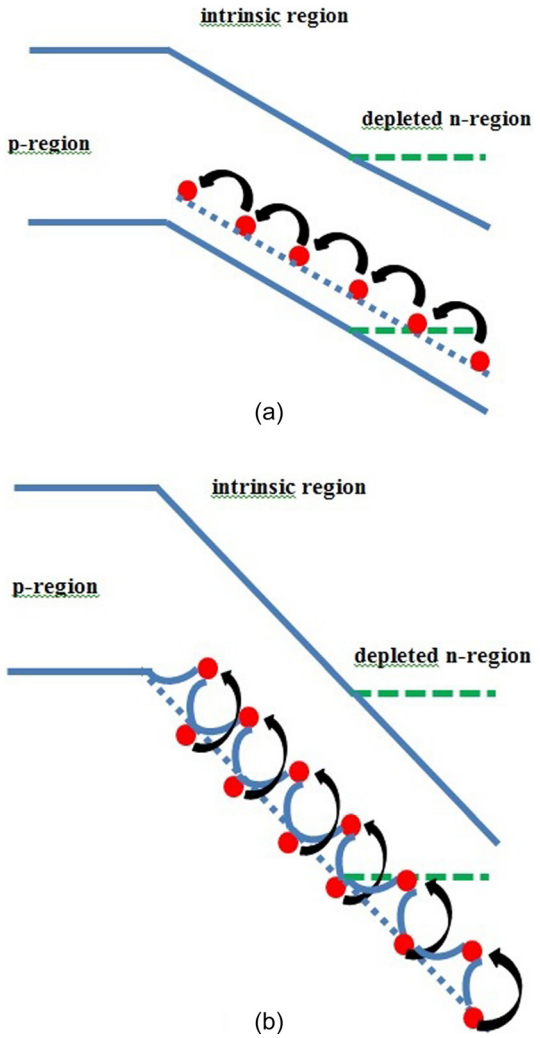

FIG. 2. Band diagram at (a) low electric fields and (b) high electric fields. Holes are represented with red circles and the green color shows the conduction and valence bands of the n-region before it is depleted. Holes are injected from the cathode contact. In the case of hopping conduction, the hole energies are lower than the maximum energy of the potential barrier between two trapping sites, and hole transport is primarily by thermally assisted tunneling between sites. However, at higher electric fields, the barrier to thermionic emission to the valence band for holes is lowered; leading to transport dominated by PFE.

field enhanced thermal emission, this mechanism is often observed at high temperatures and high electric fields.[32] The current associated with PFE is given by[34]

$$I = \frac{S\sigma}{t} V \exp\left(-\frac{q\phi_B}{kT}\right) \exp\left(\frac{q}{kT}\sqrt{\frac{qV}{\pi\varepsilon_i t}}\right), \quad (1)$$

where V is the applied voltage, S is the total wafer cross-sectional area, t is the total thickness of the layer which the TDs span, in this case the i-layer of the PIN diode structure and the depletion regions of the n- and p-regions. ϕ_B is the barrier height for carrier emission from trapped states, k is Boltzmann's constant, T is the absolute temperature, q is the electron charge, and ε_i is the optical (high-frequency) permittivity of diamond. During the PFE process, since the carrier transit time to overcome the barrier height is shorter than the dielectric relaxation time of diamond, there is no sufficient time for the medium to be polarized; thus, the optical (high-frequency) permittivity is used, which is smaller than the low-frequency one in which more polarization mechanisms contribute to the total polarization.[31] In addition, σ is the conductivity in the continuum states and is assumed to be

$$\sigma = \frac{q\mu N_{TD}}{t}, \quad (2)$$

where N_{TD} is the threading dislocation density (#cm^{-2}) and μ is the carrier mobility in the continuum. For an increase in applied voltage, the barrier against carrier tunneling to the conduction/valence band is lowered. This increases the probability of hopping from/to threading dislocation sites and thereby increases the conductivity due to the PFE mechanism. Equation (1) can be rewritten as

$$ln\left(\frac{I}{V}\right) = b(T) + m(T)\sqrt{V}, \quad (3)$$

where m and b are temperature-dependent parameters, which can be expressed as

$$m(T) = \frac{q}{KT}\sqrt{\frac{q}{\pi\varepsilon_i t}}, \quad (4)$$

$$b(T) = ln\left(\frac{S\sigma}{t}\right) - \frac{q\phi_B}{KT}. \quad (5)$$

From $m(T)$ in Eq. (4), the total thickness of the i-layer (t) can be extracted. Once t is determined, the threading dislocation density (N_{TD}) and the barrier height (ϕ_B) can be obtained from Eq. (5). In the next paragraph, the temperature analysis of experimental data will be addressed.

At low electric fields, holes as the dominant carriers in the leakage current of diamond-based PIN diodes cannot overcome the maximum energy of the potential barrier between two trapping sites; thus, hopping conduction via thermally assisted tunneling is the dominant transport mechanism. The model for hopping conduction is given by[25]

$$I = \frac{SqaN_{TD}\nu}{t} \exp\left(-\frac{qE_a}{kT}\right)\left\{\exp\left(\frac{qaV}{tkT}\right) - 1\right\}, \quad (6)$$

where a is the hopping distance, ν is the thermal vibration frequency of holes at trap sites, and E_a is the activation energy.

Figure 3(a) shows a typical set of semilogarithmic reverse bias experimental I-V characteristics of a diamond PIN diode in the temperature range of 323–423 K. A total of 4 samples were compared: D300 (round cross-section with a diameter of 280 μm), D100 (round cross-section with a diameter of 80 μm), L400 (square cross-section of 380 μm × 380 μm), and L150 (square cross-section of 130 μm × 130 μm), respectively, with similar current-voltage characteristics. As shown in Fig. 3 for one device, D300, the current increases monotonically with increasing temperature. For small reverse bias conditions and currents, the current is noisy due to the experimental measurement limits. In order to interpret the observed electrical characteristics shown in Fig. 3, a fit to the data is performed using

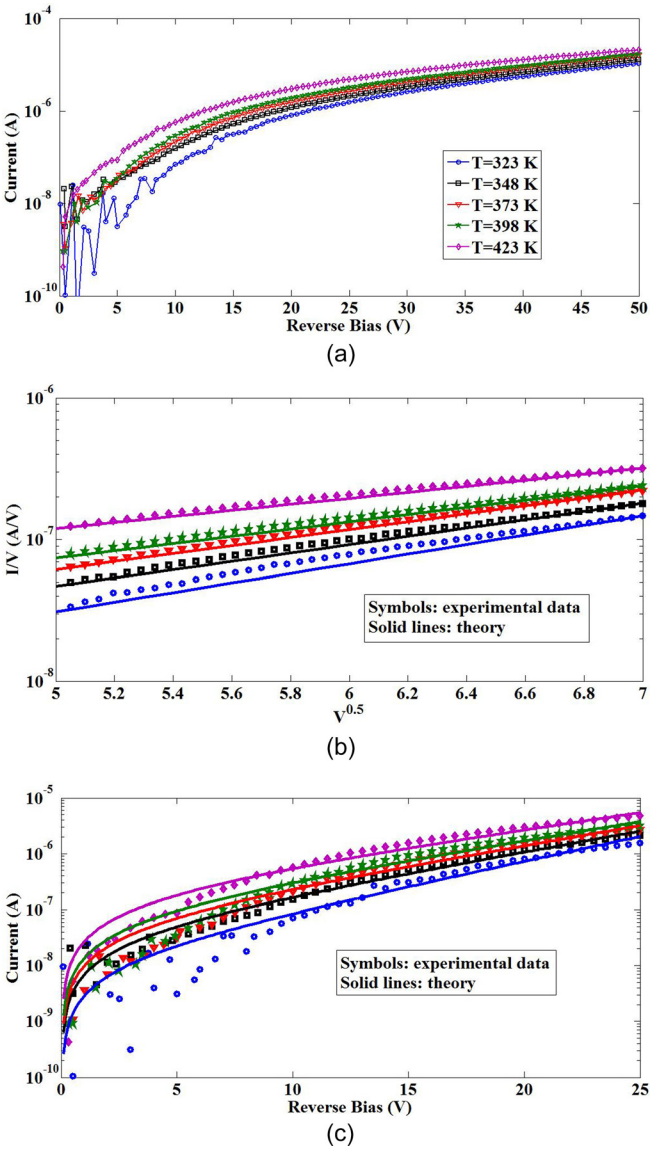

FIG. 3. (a) Experimental I-V characteristics for the D300 sample while temperature varies from 323 K to 423 K. (b) I/V curves of the experimental data of the D300 sample as functions of the square root of the applied reverse bias voltages are presented with symbols while solid lines represent theory results based on Eq. (3) (PFE mechanism). (c) Current curves of the experimental data of the D300 sample as functions of the applied reverse bias voltages are presented with symbols while solid lines represent theory results based on Eq. (6) (hopping conduction mechanism).

Eqs. (3) and (6) in Figs. 3(b) and 3(c), respectively. Figure 3(b) shows a plot of *ln(I/V)* versus $\sqrt{V}$ and the corresponding fit using Eq. (3) with *b* and *m* as fitting parameters. As shown in Fig. 3(b), good agreement is obtained, which is indicative of the dominance of the Poole-Frenkel transport at high electric fields. At low electric fields as shown in Fig. 3(c), a plot of *ln(I)* versus *V* indicates that hopping conduction as described by Eq. (6) is in good agreement with the experimental data. Below, we discuss in details the parameters used in the fits of Figs. 3(b) and 3(c).

In order to extract the total effective thickness of the *i*-layer (*t*), the threading dislocation density (N_{TD}), and the barrier height (ϕ_B), the *m* and *b* parameters [defined in Eqs. (4) and (5), respectively] extracted from data for all four samples as a function of temperature are shown in Fig. 4. As shown in Fig. 4, both *m* and *b* show a 1/T dependence consistent with PFE. In extracting the TD density and barrier height, the hole mobility (μ) is assumed to be $1000\,cm^2/V\,s$ in the low-doped *i*-layer.[35,36] In Fig. 4, the solid line fits of the experimental data exhibit the temperature dependence expected for the PFE mechanism [Eqs. (4) and (5)]. A total thickness of the *i*-layer of $2.38 \pm 1.25\,\mu m$ and an emission barrier height of $0.278 \pm 0.04\,eV$ are obtained from the slopes of *m(T)* and *b(T)*, respectively. $2.38\,\mu m$ and $1.25\,\mu m$ are the mean and standard deviation of the total *i*-layer thickness for all four devices while 0.278 eV and 0.04 eV are the mean and standard deviation of the emission barrier heights for the devices. The *i*-layer thickness compares well with the experimentally measured thickness from capacitance-voltage (C-V) measurement plus thickness of depleted n- and p-regions. In addition, the extracted emission barrier height of 0.278 eV is compatible with similar studies for other materials where Poole-Frenkel emission is the dominant transport mechanism.[20–22,31,34] The threading dislocation density ($\#cm^{-2}$) can be determined from the y-intercept of Eq. (5) in which the conductivity (σ) is defined in Eq. (2). By substituting values for the related parameters, a threading dislocation density of $5.45 \times 10^4 \pm 1.44 \times 10^4\,cm^{-2}$ is obtained in which $5.45 \times 10^4\,cm^{-2}$ and $1.44 \times 10^4\,cm^{-2}$ are the mean and standard deviation of the threading dislocation density for all four devices. The threading dislocation density is in good agreement with the order of magnitude values reported in previous works on good quality CVD diamond films.[37,38] Compared with diamond, other wide bandgap materials such as GaN and SiC have threading dislocation densities which change depending on their quality and fabrication process. For the case of GaN, conventional metal-organic chemical vapor deposition (MOCVD) hetero-epitaxy results in a high TD density in the range of 10^7–$10^{10}\,cm^{-2}$, the epitaxial lateral overgrowth (ELOG) technique decreases the TD densities to 10^6–$10^7\,cm^{-2}$, and the GaN epilayer on the near-strain-free GaN compliant buffer suppresses the TD density as low as $10^5\,cm^{-2}$.[39] On the other hand, the TD density for SiC varies between $10^3\,cm^{-2}$ and $10^4\,cm^{-2}$.[40]

The important parameters for hopping conduction are obtained assuming that the frequency of thermal vibration of holes at trap sites (ν) is fixed at 5.1×10^{13} Hz (Ref. 41) and the total thickness of the *i*-layer is the same as that for PFE ($2.38\,\mu m$). From the slope of *ln(I)* versus *V* in the curve fits of Fig. 3(c), the hopping distance (*a*) is extracted to be 12.4 ± 0.61 nm in which 12.4 nm and 0.61 nm are the mean and standard deviation of the hopping distance for all four devices. With the known hopping distance, the activation energy (E_a) of 0.227 ± 0.03 eV is taken out from the slope of Arrhenius plots in Fig. 5. The values of 0.227 eV and 0.03 eV are the mean and standard deviation of the activation energy for all seven curves in Fig. 5. The threading dislocation density is also obtained to be $4.40 \times 10^4 \pm 1.26 \times 10^4\,cm^{-2}$ ($4.40 \times 10^4\,cm^{-2}$ and $1.26 \times 10^4\,cm^{-2}$ are the mean and standard deviation of the threading dislocation for all seven curves in Fig. 5) from the y-intercept of Arrhenius plots in Fig. 5. The threading dislocation density values obtained for hopping conduction are in the range of the threading dislocation density extracted based on the PFE mechanism ($5.45 \times 10^4 \pm 1.44 \times 10^4\,cm^{-2}$). As mentioned before, tunneling between two trapping sites for hopping conduction of holes does not need to overcome the maximum barrier height toward the valence band, and thus, the

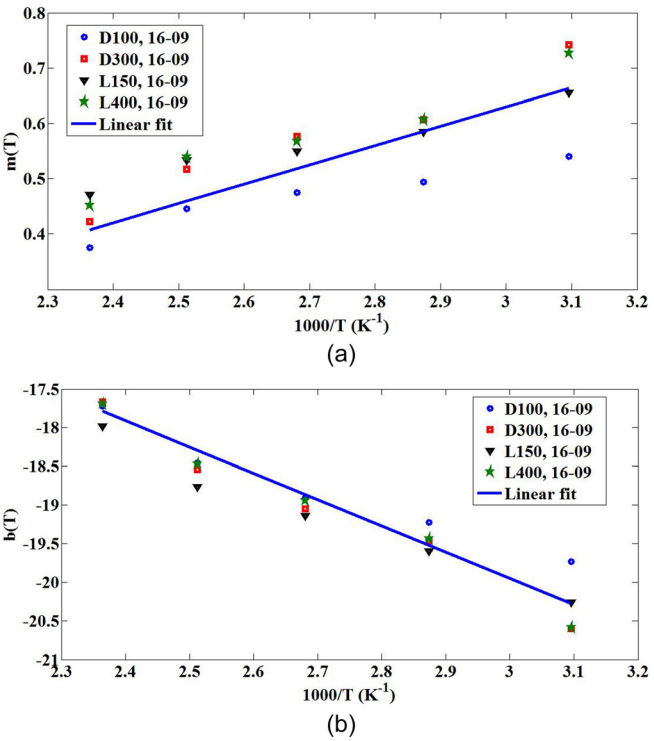

FIG. 4. The extracted PFE parameters from experimental data: (a) *m* and (b) *b* as functions of temperature. The solid blue lines represent linear fittings of extracted *m* and *b* parameters.

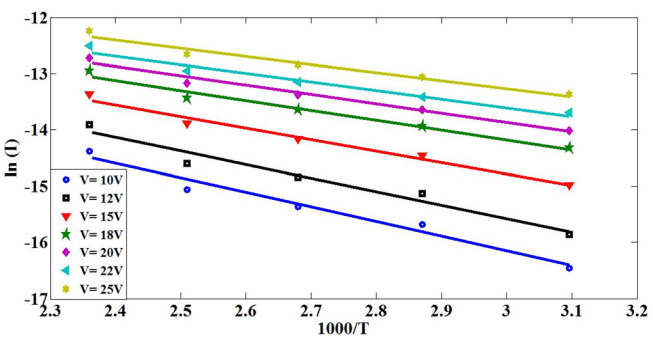

FIG. 5. Arrhenius plot of hopping conduction at low electric fields in which symbols are experimental data and solid lines are fitting curves.

activation energy of the hopping conduction mechanism (0.227 ± 0.03 eV) is lower than the barrier height of the PFE mechanism (0.278 ± 0.04 eV).

Conduction through threading dislocations (TDs) in diamond-based PIN diodes has been analyzed at different temperatures based on electrical conduction through TDs described by hopping conduction and Poole-Frenkel emission (PFE) mechanisms at low and high electric fields, respectively. These models provide an excellent fit to the leakage current as a function of the temperature and bias. From the PFE equations, the barrier height of TDs, total effective thickness of the *i*-layer, and TD density of diamond were extracted from experimental data. In addition, the hopping distance, activation energy, and TD density were extracted from experimental data based on the hopping conduction equation. The TD densities extracted from PFE and hopping conduction are in the same range.

The authors would like to acknowledge the ARPA-E SWITCHES program under Grant No. "DE-AR0000453."

[1]X. Q. Shen, H. Matsuhata, and H. Okumura, Appl. Phys. Lett. **86**, 021912 (2005).
[2]H. Amini Moghadam, S. Dimitrijev, J. Han, D. Haasmann, and A. Aminbeidokhti, IEEE Trans. Electron Devices **62**(8), 2670–2674 (2015).
[3]S. Koizumi, C. E. Nebel, and M. Nesladek, *Physics and Applications of CVD Diamond* (Wiley-VCH, 2008).
[4]J. Pernot, P. N. Volpe, F. Omnes, P. Muret, V. Mortet, K. Haenen, and T. Teraji, Phys. Rev. B **81**, 205203 (2010).
[5]T. R. Anthony, W. F. Banholzer, J. F. Fleischer, L. Wei, P. K. Kuo, R. L. Thomas, and R. W. Pryor, Phys. Rev. B **42**, 1104 (1990).
[6]L. Wei, P. K. Kuo, R. L. Thomas, T. R. Anthony, and W. F. Banholzer, Phys. Rev. Lett. **70**, 3764 (1993).
[7]J. Liu, H. Ohsato, X. Wang, M. Liao, and Y. Koide, Sci. Rep. **6**, 34757 (2016).
[8]S. A. O. Russell, S. Sharabi, A. Tallaire, and D. A. J. Moran, IEEE Electron Device Lett. **33**, 1471 (2012).
[9]T. Iwasaki, Y. Hoshino, K. Tsuzuki, H. Kato, T. Makino, M. Ogura, D. Takeuchi, T. Matsumoto, H. Okushi, S. Yamasaki, and M. Hatano, Appl. Phys. Express **5**, 091301 (2012).
[10]P.-N. Volpe, P. Muret, J. Pernot, F. Omnes, T. Teraji, Y. Koide, F. Jornard, D. Planson, P. Brosselard, N. Dheilly, B. Vergne, and S. Scharnholz, Appl. Phys. Lett. **97**, 223501 (2010).
[11]Y. Hoshino, H. Kato, T. Makino, M. Ogura, T. Iwasaki, M. Hatano, and S. Yamasaki, Phys. Status Solidi A **209**, 1761 (2012).
[12]C. J. H. Wort and R. S. Balmer, Mater. Today **11**, 22 (2008).
[13]H. Sumiya and K. Tamasaku, Jpn. J. Appl. Phys. **51**, 09102 (2012); available at http://iopscience.iop.org/1347-4065/51/9R/090102.
[14]A. T. Collins, H. Kanda, and H. Kitawaki, Diamond Relat. Mater. **9**, 113 (2000).
[15]P. M. Martineau, M. P. Gaukroger, K. B. Guy, S. C. Lawson, D. J. Twitchen, I. Friel, J. O. Hansen, G. C. Summerton, T. P. G. Addison, and R. Burns, J. Phys.: Condens. Mater. **21**, 364205 (2009).
[16]N. Tatsumi, K. Tamasaku, T. Ito, and H. Sumiya, J. Cryst. Growth **458**, 27–30 (2017).
[17]J. W. P. Hsu, M. J. Manfra, D. V. Lang, S. Richter, S. N. G. Chu, A. M. Sergent, R. N. Kleiman, L. N. Pfeiffer, and R. J. Molnar, Appl. Phys. Lett. **78**, 1685 (2001).
[18]F. Iucolano, F. Roccaforte, F. Giannazzo, and V. Raineri, J. Appl. Phys. **104**, 093706 (2008).
[19]O. Mitrofanov and M. Manfra, Appl. Phys. Lett. **84**, 422 (2004).
[20]C. Xu, J. Wang, H. Chen, F. Xu, Z. Dong, Y. Hao, and C. P. Wen, IEEE Electron Device Lett. **28**, 942 (2007).
[21]H. Zhang, E. J. Miller, and E. T. Yu, J. Appl. Phys. **99**, 023703 (2006).
[22]C. Couso, V. Iglesias, M. Porti, S. Claramunt, M. Nafria, N. Domingo, A. Cordes, and G. Bersuker, IEEE Electron Device Lett. **37**, 640–643 (2016).
[23]S. D. Ganichev, E. Ziemann, and W. Prettl, Phys. Rev. B **61**, 10361 (2000).
[24]F.-C. Chiu, C.-Y. Lee, and T.-M. Pan, J. Appl. Phys. **105**, 074103 (2009).
[25]S. Zaima, T. Furuta, Y. Koide, and Y. Yasuda, and J. Electrochem. Soc. **137**, 2876 (1990).
[26]M. Dutta, F. A. M. Koeck, R. Hathwar, S. Goodnick, R. J. Nemanich, and S. Chowdhury, IEEE Electron Device Lett. **37**, 1170 (2016).
[27]M. Dutta, F. A. M. Koeck, W. Li, R. J. Nemanich, and S. Chowdhury, "High voltage diodes in diamond using (100)- and (111)- substrates," IEEE Electron Device Lett. **38**, 600 (2017).
[28]A. R. Lang, Diamond Relat. Mater. **2**, 106 (1993).
[29]Y. Kato, H. Umezawa, H. Yamaguchi, and S. Shikata, Diamond Relat. Mater. **29**, 37 (2012).
[30]S. Masuya, K. Hanada, T. Uematsu, T. Moribayashi, H. Sumiya, and M. Kasu, Jpn. J. Appl. Phys. **55**, 04303 (2016); available at http://iopscience.iop.org/1347-4065/55/4/040303.
[31]F.-C. Chiu, Adv. Mater. Sci. Eng. **2014**, 578168 (2014).
[32]J. Frenkel, Phys. Rev. **54**, 647 (1938).
[33]R. L. Angle and H. E. Talley, IEEE Trans. Electron Devices **25**, 1277–1283 (1978).
[34]H. Schroeder, J. Appl. Phys. **117**, 215103 (2015).
[35]J. Pernot, C. Tavares, E. Gheeraert, E. Bustarret, M. Katagiri, and S. Koizumi, Appl. Phys. Lett. **89**, 122111 (2006).
[36]J. Pernot and S. Koizumi, Appl. Phys. Lett. **93**, 052105 (2008).
[37]S. Shikata, Diamond Relat. Mater. **65**, 168–175 (2016).
[38]A. Tallaire, T. Ouisse, A. Lantreibecq, R. Cours, M. Legros, H. Bensalah, J. Barjon, V. Mille, O. Brinza, and J. Achard, Cryst. Growth Des. **16**, 2741–2746 (2016).
[39]H.-Y. Shih, M. Shiojiri, C.-H. Chen, S.-F. Yu, C.-T. Ko, J.-R. Yang, R.-M. Lin, and M.-J. Chen, Sci. Rep. **5**, 13671 (2015).
[40]H. Fujiwara, H. Naruoka, M. Konishi, K. Hamada, T. Katsuno, T. Ishikawa, Y. Watanabe, and T. Endo, Appl. Phys. Lett. **100**, 242102 (2012).
[41]R. Hathwar, M. Dutta, F. A. M. Koeck, R. J. Nemanich, S. Chowdhury, and S. M. Goodnick, J. Appl. Phys. **119**, 225703 (2016).